Available online at BCREC website: https://bcrec.id

Bulletin of Chemical Reaction Engineering & Catalysis, 18 (3) 2023, 506-520

Research Article

Synthesis of CuO, ZnO and SnO_2 Coupled TiO_2 Photocatalyst Particles for Enhanced Photodegradation of Rhodamine B Dye

Amna Jwad Kadem, Zhuang Min Tan, Nanthini Mohana Suntharam, Swee-Yong Pung, Sivakumar Ramakrishnan*

School of Materials and Mineral Resources Engineering, Engineering Campus, Universiti Sains Malaysia, 14300 Nibong Tebal, Penang, Malaysia.

Received: 7th August 2023; Revised: 3rd October 2023; Accepted: 3rd October 2023
Available online: 4th October 2023; Published regularly: October 2023

Abstract

Environmental pollution is a global problem and dye pollution is one of the major factors. TiO_2 shows promising photocatalytic properties that can degrade organic pollutants such as dye under ultraviolet (UV) irradiation. However, TiO_2 possesses some disadvantages such as a wide band gap and a high recombination rate of electron-hole pairs. Coupling TiO_2 with various metal oxides can enhance photocatalytic properties. In this work, photodeposition (reduction of metal ions on TiO_2) followed by the thermal oxidation method were used for the coupling of TiO_2 with CuO, ZnO, or SnO_2 under various methanol concentrations (25 vol% or 50 vol%) and deposition duration (1 h or 3 h) to observe the effect of these parameters on the photocatalytic degradation activity on Rhodamine B (RhB) dye (up to 90 min). The rate constant of the photodegradation reaction (k) has improved from 0.0141 min^{-1} (uncoupled TiO_2) to 0.0151~0.0368 min^{-1}. Overall, CuO/TiO_2 and SnO_2/TiO_2 samples have shown similar photocatalytic properties (average rate constants of 0.0341 min^{-1} and 0.0327 min^{-1}, respectively), and both performed better than ZnO/TiO_2 in terms of RhB photodegradation (average rate constants of 0.0197 min^{-1}). The difference in photocatalytic performance can be explained by the bandgap of metal oxides and their relative band positions with TiO_2. Lastly, CuO/TiO_2 (50 vol%, 3 h) and SnO_2/TiO_2 (50 vol%, 3 h) have shown the best photocatalytic properties respectively due to a longer deposition time and higher concentration methanol, resulting in more deposited materials.

Keywords: Photodegradation; Photodeposition; TiO_2; CuO; SnO_2; Photocatalyst

How to Cite: A.J. Kadem, Z.M. Tan, N.M. Suntharam, S.Y. Pung, S. Ramakrishnan (2023). Synthesis of CuO, ZnO and SnO_2 Coupled TiO_2 Photocatalyst Particles for Enhanced Photodegradation of Rhodamine B Dye. *Bulletin of Chemical Reaction Engineering & Catalysis*, 18(3), 506-520 (doi: 10.9767/bcrec.19532)

Permalink/DOI: https://doi.org/10.9767/bcrec.19532

1. Introduction

Environmental pollution is becoming an urgent global problem with the rapid development of industry. The textile industry, which involves the use of dyes that are difficult to degrade, is one of the major contributors to environmental pollution. More than 10,000 types of dyes are being used in the textile industry. During the production of textiles, the remaining dyes that are not being incorporated into the fabric will become waste. If the waste is not being treated prior to discharge, it can pollute the environment. Although most of the colors can stay on the fabrics, 30 to 40 percent of the dyes will be washed out directly into the environment or into the drainage system [1]. The difficulty of treating dye-containing effluents may become greater after they have entered the environment because the dyes have a synthetic origin and com-

* Corresponding Author.
Email: srsivakumar@usm.my (S. Ramakrishnan)

plex molecular structure, which makes them more stable and less biodegradable in that case. On top of that, the wastewater can be absorbed by terrestrial and aquatic plants. The harmful chemicals can be passed to animals in the food chain and eventually to humans. The toxic effects of dyes range from cancer and allergies to humans, to growth inhibitions of microscopic organisms and plants. Not only that, but extensive water pollution from dyes can also cause damage to the country's economy due to the generally expensive pollution clean-up procedure.

Until today, several traditional approaches have been adopted to address organic pollution worldwide: membrane separation [2], flocculation-condensation [3], adsorption [4], oxidation or ozonation [5] and reverse osmosis [6]. However, these approaches are unable to remove organic pollutants completely or effectively [7]. Photocatalytic degradation of wastewater is a promising way owing to efficiency, green, environmental compatibility, and convenience. Photocatalytic reaction is a heterogeneous reaction that occurs on the catalyst surface to accelerate the conversion of light energy into chemical energy, including excitation, redox reaction and recombination, and to achieve the potential balance between the Fermi energy level of the catalyst and the surface adsorbents [7]. In general, the photocatalytic reaction can be broken down into 4 steps: (1) photon irradiation on the photocatalyst to induce photogeneration of electron-hole pairs, (2) charge carrier separation and migration to the surface of the photocatalyst, (3) reduction/oxidation reaction by the charge carriers, and (4) recombination of charge carriers in the bulk or on the surface of photocatalyst. These four steps are complementary, and the thermodynamics and kinetics of these processes determine the efficiency of a given photocatalyst [8]. In step 3, the generated electron is used for reducing an acceptor whereas the generated hole is used for oxidation of donor molecules, hence a photocatalyst provides both oxidation and reduction environment simultaneously [9].

Generally, photocatalysts that are used in photocatalytic degradation are made up of semiconductor materials. A photocatalyst is a material that can convert light energy into chemical energy by absorbing light, bringing itself to a higher energy level to provide energy to a reacting substance and make a chemical reaction to occur or change the rate of a chemical reaction [9,10]. On the other side, TiO_2 as a semiconductor photocatalyst has drawn the attention of many nanomaterial researchers due to its high potential for the energy sector, as well as for environmental protection applications which is the focus of this project. Besides, due to its other attractive qualities, such as good optical properties, low cost, high photocatalytic activity, chemical stability, and non-toxicity, TiO_2 is also being used in many other areas such as disinfectants and antibacterial agents, self-cleaning surfaces, food and pharmaceutical additives, pigments, sensors and many more [11]. One of the advantages of TiO_2 over other semiconductors as a photocatalyst is that it allows simultaneous oxidation of hydrogen and reduction of oxygen due to its electronic structure, where the bottom of its conduction band (CB) is more negative than the reduction potential of H^+/H_2 (E_{NHE} = 0.00V), and the top of its valence band (VB) is more positive than the oxidation potential of O_2/H_2O (E_{NHE} = 1.23 V) [12]. However, TiO_2 possesses certain limitations in terms of photocatalytic performance and bandgap. The drawback of TiO_2 as a photocatalyst is its wide bandgap, meaning that pure TiO_2 can only absorb light with a wavelength in the UV range or shorter. Due to their wide band gap, TiO_2 can only absorb less than 5% of solar energy, making the development of solar technologies that are based on TiO_2 a challenge [13]. Rapid recombination of these electron-hole pairs is another challenge for TiO_2 photocatalysts [14].

To enhance the photocatalytic activity of TiO_2, heterojunctions should be established, where TiO_2 can be coupled with other components such as metals or semiconductors. Coupled TiO_2 can be synthesized in various ways such as the sol-gel method [15], hydrothermal method [16], impregnation method [17], photo deposition method [18]. Photo deposition and thermal oxidation were used to achieve coupling because it is a relatively cheap and straightforward method [19]. Three important TiO_2 polymorphs can be prepared without using special synthesis conditions. Those are anatase, rutile and brookite. The rutile phase is thermodynamically most stable TiO_2 polymorph at all temperatures and pressures below 60 kPa, but the Gibbs free energy differences between rutile, brookite and anatase are small (around 4 to 20 $kJ.mol^{-1}$), so brookite and anatase can be obtained as metastable phases [12,20]. At low temperatures, the transformation of anatase to rutile occurs at an insignificant rate; however, at 600 °C, the transformation takes place in pure TiO_2 by surface nucleation and growth mechanism [21]. Therefore, another research also stated in their review on TiO_2 that after low-temperature treat-

ments, anatase or anatase-brookite mixtures will be obtained, although poorly crystallized or amorphous TiO_2 may constitute a large proportion of it [22]. The rutile phase on the other hand usually starts to appear with following calcination at moderate temperatures (300-500 °C) and becomes the predominant phase after high-temperature treatments (>600 °C) [22].

Three metal oxides were selected in this work based on their bandgap relative to anatase TiO_2 (3.2 eV). Firstly, copper oxide (CuO) has a smaller bandgap than TiO_2 (1.6 eV); tin oxide (SnO_2) has larger bandgap than TiO_2 (3.6 eV); zinc(II) oxide (ZnO) has a bandgap that is almost similar to TiO_2 (3.3 eV) [23]. The purpose was to study how the relative bandgap affects the outcome of photocatalytic properties. Photo deposition followed by thermal oxidation was used to achieve coupling because it is a relatively cheap and straightforward method. The photo deposition method works by illuminating light with sufficient energy on the photocatalyst, the photoexcited electrons will reduce metal cations from the precursor to produce metal nanoparticles on the surface of the photocatalyst. Since photodeposition method provides the metal nanoparticles on the reductive site of the photocatalyst surface, the metal nanoparticles formed can further accelerate the reductive reaction [24].

The thermal oxidation method is used to convert metal into their desired oxide form by subjecting the metal to heat in an oxygen-containing environment. The simplest form of oxidation of a metal surface may occur even at room temperature to form a thin layer of oxide in the presence of oxygen in air. But in most cases, the process will then slow down and stop after the oxide layer has reached a few nanometers thick due to the insufficient energy of oxygen atoms to diffuse through the already formed oxide layer [25–28]. However, in thermal oxidation, the metal is subjected to heat to control the diffusion process and chemical reactivity of oxygen atoms with the metal atoms. In thermal oxidation, there are usually more than one form of oxides for every metal, depending on the annealing parameters such as temperature, duration, and partial pressure of oxygen in the environment [29]. In this work, the desired oxide phases are CuO, ZnO, and SnO_2. A generalized set of parameters was used for the thermal oxidation of all types of samples to maintain the consistency of the TiO_2 phase across all samples since the TiO_2 phases can be one of the factors affecting the overall photocatalytic performance. The novelty of this research lies in the systematic investigation of TiO_2 coupled with different metal oxides, considering the impact of synthesis parameters, and comparing their photocatalytic performance for degrading RhB dye. This work is important because it addresses the pressing issue of environmental pollution caused by dye contaminants, offering insights into improving photocatalytic technologies for wastewater treatment and pollution control. Additionally, it contributes to the understanding of how the choice of metal oxide and synthesis conditions can influence the efficiency of photocatalytic processes, potentially guiding future research in this field.

2. Materials and Method

2.1 Materials

TiO_2 particles (Merck, 99.5%) were used to couple with CuO, ZnO, and SnO_2. The precursors for the photodeposition of metals were copper(II) acetate (($Cu(CH_3COO)_2$), Pluka, 99.0%), zinc acetate (($Zn(CH_3COO)_2$), Merck, 99.99%), and tin(II) chloride dehydrate (($SnCl_2.2H_2O$), Merck, 98%). The hole scavenger used for photodeposition was methanol (CH_3OH, Merck, 99.9%). Rhodamine B solution ($C_{28}H_3ClN_2O_3$, Merck) was used for the photodegradation process by the metal oxide coupled TiO_2 particles. Propanol (C_3H_8O, Merck, 99.8 %) was used as a general cleaning solution.

2.2 Preparative Procedure

The design of experiment method was used to optimize two variables which are the concentration of methanol and UV irradiation. To couple the TiO_2 particles with metal, firstly the amount of metal ion precursor copper (ii) acetate (0.3632 g), zinc acetate (0.3668 g), and tin (ii) chloride (0.3792 g) was prepared and mixed with 500 mL / 750 mL of deionized water in a beaker, which is then added with 250 mL / 500 mL of methanol to obtain the respective metal ion solution of 2 mM concentration and methanol concentration of 25 vol% / 50 vol%. The mixture was stirred for 15 min. Then, 2 g of TiO_2 particles were prepared and added into the solution, and stirred in a dark condition for 30 min. Next, the mixture was stirred under UV radiation for 1 h / 3 h. The metal coupled TiO_2 particles were then separated from the metal ion solution by the centrifuge (Hettich ROTOFIX 32A) and dried in an oven under 90 °C for 24 h. Subsequently, annealing was carried out in the open air using a tube furnace for thermal oxidation of the photodeposited metal. Figure 1 shows the temperature profile of the

annealing process. The particles were heated to 600 °C by 10 °C/min in open air from room temperature. After the soaking period, the particles were allowed to cool down to room temperature. Since various combinations of the two parameters were used, the denotations of each sample are listed in Table 1.

2.3 Characterization

2.3.1 Structural and morphological

The synthesized metal oxide coupled TiO_2 particles were subjected to several characterization techniques to obtain various information about the particles. The particles were examined by field emission scanning electron microscopy (FESEM, FEI Quanta 650 FEG SEM), energy dispersive x-ray spectrophotometer (EDX) that couples with FESEM to analyze the sample's elemental composition, and X-ray diffraction (XRD Bruker D8 diffractometer).

2.3.2 Photocatalytic properties

Rhodamine B (RhB) dye solution was chosen in the photocatalytic study. The initial concentration of RhB dye solution (C_0) was prepared at 5 ppm. This was done by mixing 0.005 g of RhB dye powder with 1000 mL distilled water followed by stirring for 30 min. Prior to testing, two control samples were prepared using dye containing 0.10 g of metal oxide coupled TiO_2 particles before degradation and another sample with deionized water. For degradation, 0.10 g of the metal oxide coupled TiO_2 photocatalyst particles was firstly dispersed into 150 mL of one of the dye solutions and stirred for 30 min in dark condition to ensure saturation of the dye on the photocatalyst surface. Then, the mixture was exposed to UV light irradiation by UV lamp of 150 lm/W, and 1.5 mL of the mixture was pipetted out into a cuvette every 15 min until 90 min was reached. The absorbance of the RhB solution in different cuvettes was measured using wavelength, λ from the range of 400 to 700 nm. A UV-visible spectrophotometer (UV-Visible Varian Cary 50) was used to measure the absorbance (A) with a UV light wavelength range of 190 to 400 nm and visible light wavelength range from 400 to 800 nm as the light source. It measures the transmittance, which is the ratio of the intensity of light passing through a sample (I) to the intensity of light before it passes through the sample (I_o). It is usually expressed as a percentage (%T) and it can be used to determine absorbance as shown in Equation (1).

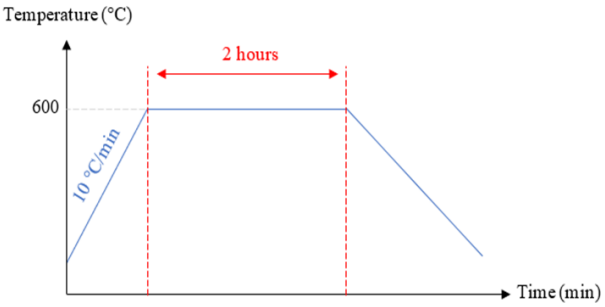

Figure 1. Temperature profile of annealing process.

$$A = -\log\left(\frac{\%T}{100\%}\right) \quad (1)$$

3. Results and Discussion

3.1 Structural and Morphological Analyses

FESEM was used to observe the surface morphology of TiO_2 particles, before and after

Table 1. Denotation of samples.

Sample Name	Methanol Concentration (vol.%)	Deposition Duration (h)
CuO/TiO_2 (25,1)	25	1
CuO/TiO_2 (50,1)	50	1
CuO/TiO_2 (25,3)	25	3
CuO/TiO_2 (50,3)	50	3
ZnO/TiO_2 (25,1)	25	1
ZnO/TiO_2 (50,1)	50	1
ZnO/TiO_2 (25,3)	25	3
ZnO/TiO_2 (50,3)	50	3
SnO_2/TiO_2 (25,1)	25	1
SnO_2/TiO_2 (50,1)	50	1
SnO_2/TiO_2 (25,3)	25	3
SnO_2/TiO_2 (50,3)	50	3

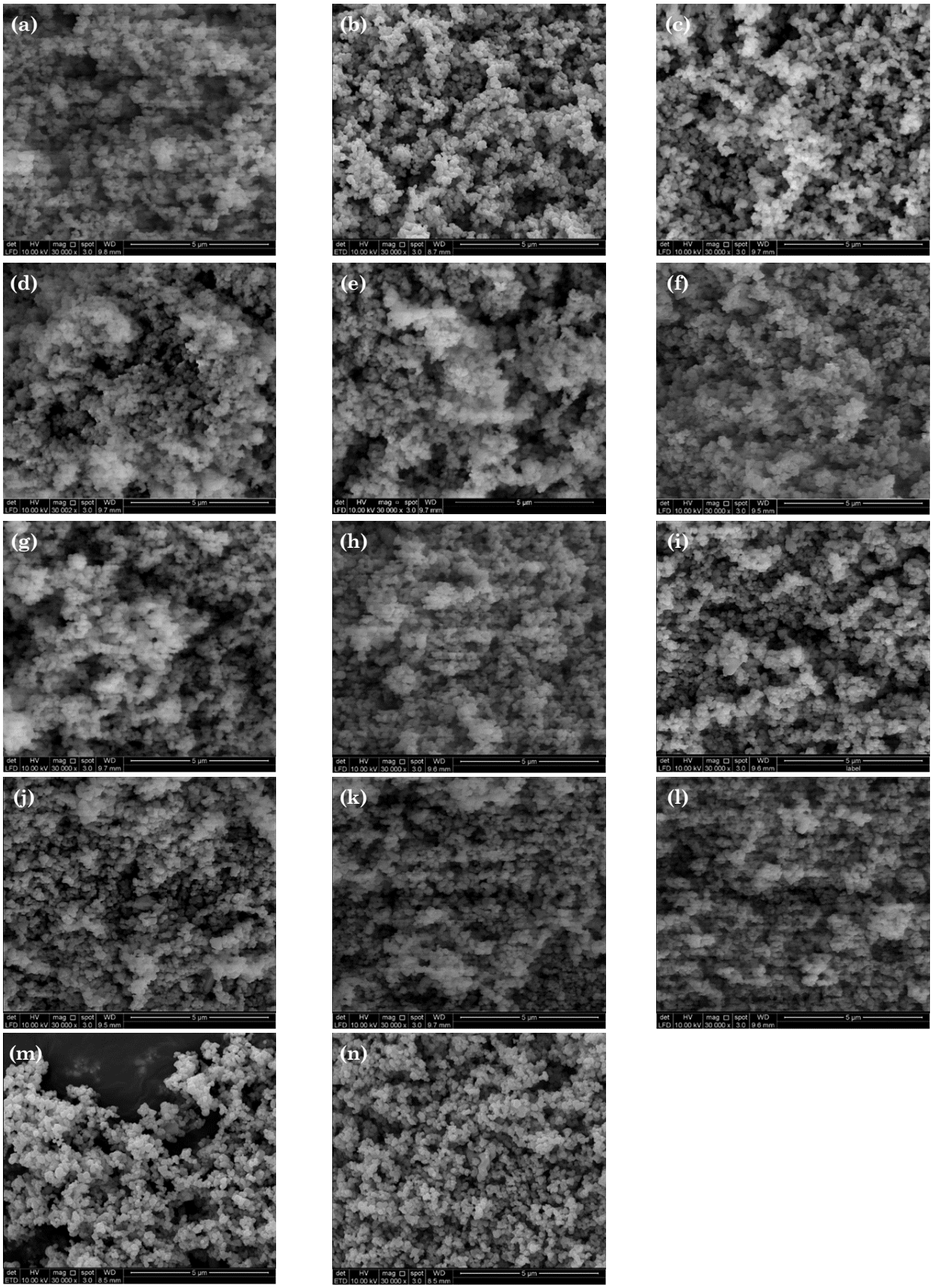

Figure 2. FESEM images of (a) TiO_2 particles before and (b) after annealing at 600 °C in ambient atmosphere for 2 h (c) CuO/TiO_2 at 25 vol%, 1 h, (d) 50 vol%, 1 h, (e) 25 vol%, 3 h, (f) 50 vol%, 3 h, (g) ZnO/TiO_2 at 25 vol%, 1 h, (h) 50 vol%, 1 h, (i) 25 vol%, 3 h, (j) 50 vol%, 3 h, (k) SnO_2/TiO_2 at 25 vol%, 1 h, (l) 50 vol%, 1 h, (m) 25 vol%, 3 h, and (n) 50 vol%, 3 h under 30kX magnification.

coupling with metal oxides. Figure 2(a-b) shows the morphology of TiO_2 particles before and after annealing at 600 °C for 2 h representatively. Similar morphologies were observed between the two samples. The average particle sizes for both samples were measured using ImageJ software with sample size = 30. The average particle size for TiO_2 particles before and after annealing was 151.12±41.67 nm and 148.56±41.89 nm respectively. To determine whether the difference in average particle size before and after annealing was significant at 95% confidence level, a two-sample *t*-test was carried out. Since the calculated *p*-value (0.813) is greater than 0.05, it can be concluded that there were no significant differences between the average particle sizes before and after annealing, and hence the annealing condition used does not affect the TiO_2 particle size and morphology. Figure 2(c-n) shows FESEM performed on metal oxide coupled TiO_2 particles such as CuO (c-f), ZnO (g-j) and SnO_2 (k-n). In terms of morphology, there were no notable differences observed between each sample, and they showed similar morphology as annealed TiO_2 particles without coupling. However, at high-temperature thermal treatments, the particle size of TiO_2 may increase and its properties may change [30]. This is undesired because the focus of this project is to determine the effect of coupling on the photocatalytic properties only, and other variables, such as changes in TiO_2 particle size and phases from heating, must not be involved. Hence, to ensure that the annealing condition used in this experiment will not affect the particle size and morphology of TiO_2, the images of pure TiO_2 particles before and after annealing was taken.

EDX analysis was carried out for elemental analysis of the coupled TiO_2 particles as shown in Figure 3. The EDX results revealed the presence of constituents from the coupled metal oxide, although in extremely small quantities, affirming the occurrence of metal oxide coupling in all samples. Besides, this explains why there were no significant increases in particle sizes nor noticeable changes in morphologies after metal oxide coupling because the amount of coupled material was too small. For CuO coupled TiO_2 particles, increasing the concentration of methanol from 25 vol% to 50 vol% while maintaining exposure duration as 1 h has increased the percentage of Cu from 0.62 at% to 0.76 at%. However, there were not many differences in the atomic percentage of Cu among CuO/TiO_2 (50,1), CuO/TiO_2 (25,3), and CuO/TiO_2 (50,3). This is likely due to photodeposition rate of Cu becoming very low as the percentage of copper has reached around 0.76 at%.

The percentages of Zn present on samples with 3 h exposure duration, which are ZnO/TiO_2 (25,3) and ZnO/TiO_2 (50,3), are great-

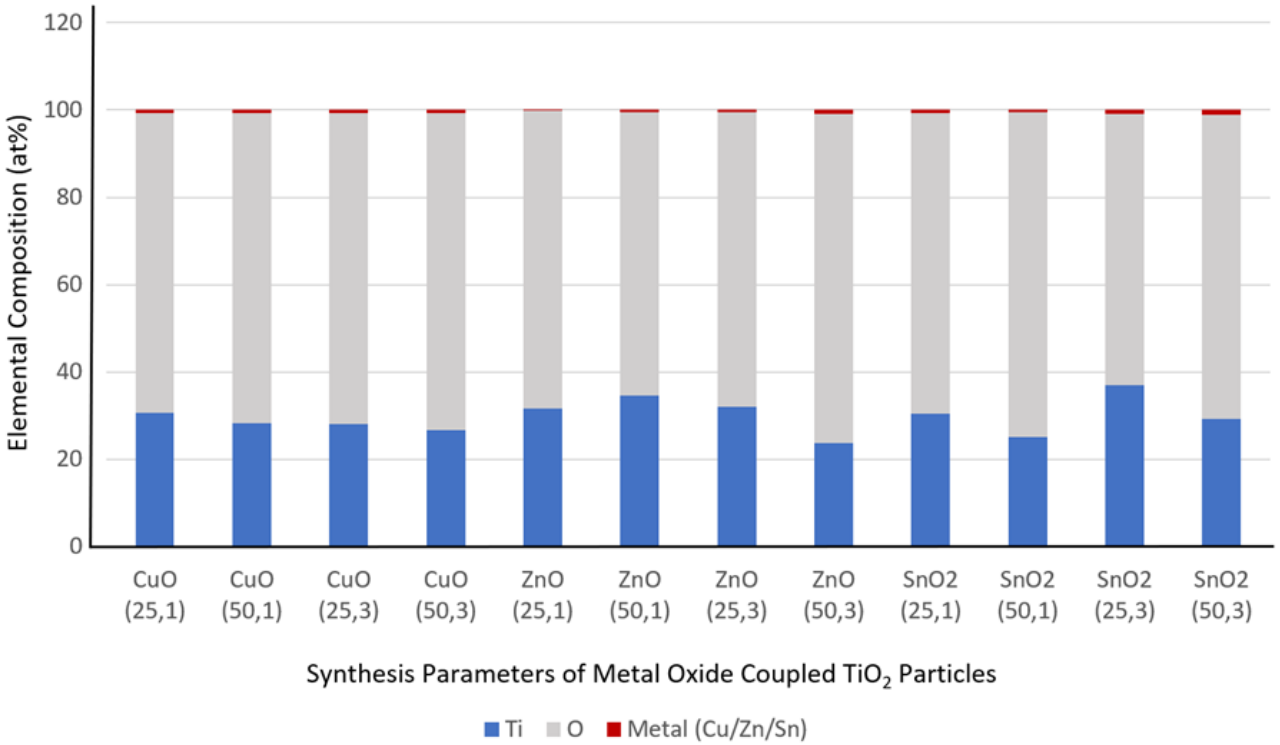

Figure 3. EDX analysis of metal oxide coupled TiO_2 particles synthesized under different parameters include (25 vol%, 1 h), (50 vol%, 1 h), (25 vol%, 3 h), and (50 vol%, 3 h).

er than samples with 1 h exposure duration, which are ZnO/TiO_2 (25,1) and ZnO/TiO_2 (50,1), because more time was given for the photodeposition of Zn atoms on TiO_2 particles to take place. Besides, for samples with the same exposure duration, the ones with a higher concentration of methanol used during photodeposition process contain a greater percentage of Zn [31]. This highlights the importance of organic hole scavengers in photoreduction of Zn ions with photoexcited TiO_2. At pH 7, the reduction potential of Zn^{2+}/Zn is more negative than the reduction potential of photogenerated electrons in the CB of TiO_2, hence Zn^{2+} cannot be directly reduced by the photogenerated electrons [32]. Instead, organic additives, in this case, methanol, can be converted into radical intermediates with strong reducing power by the photogenerated holes in VB of TiO_2 or by hydroxyl radicals, which can reduce the Zn^{2+} ions into Zn atoms [33,34]. Since the photodeposition of Zn is dependent on organic intermediates, increasing the concentration of methanol has increased the number of generated intermediates, hence speeding up the photodeposition process. Apart from that, the atomic percentage of Sn was noticeably higher in samples that have a longer exposure duration, which were SnO_2/TiO_2 (25,3) and SnO_2/TiO_2 (50,3). This is once again due to a longer time given for the photodeposition process to take place in those samples. However, despite SnO_2/TiO_2 (50,3) with 50 vol% methanol has greater Sn percentage than in SnO_2/TiO_2 (25,3) with 25 vol% methanol, SnO_2/TiO_2 (50,1) with 50 vol% methanol showed a lower percentage of Sn at 0.41 at%, compared to SnO_2/TiO_2 (50,1) with 25 vol% methanol at 0.66 at% Sn. This phenomenon indicates that the concentration of methanol might not be the prominent factor in photodeposition of Sn using UV irradiated TiO_2 particles, and the photoreduction of Sn^{2+} ions was mainly through direct electron transfer from photoexcited TiO_2 to the Sn^{2+} ions.

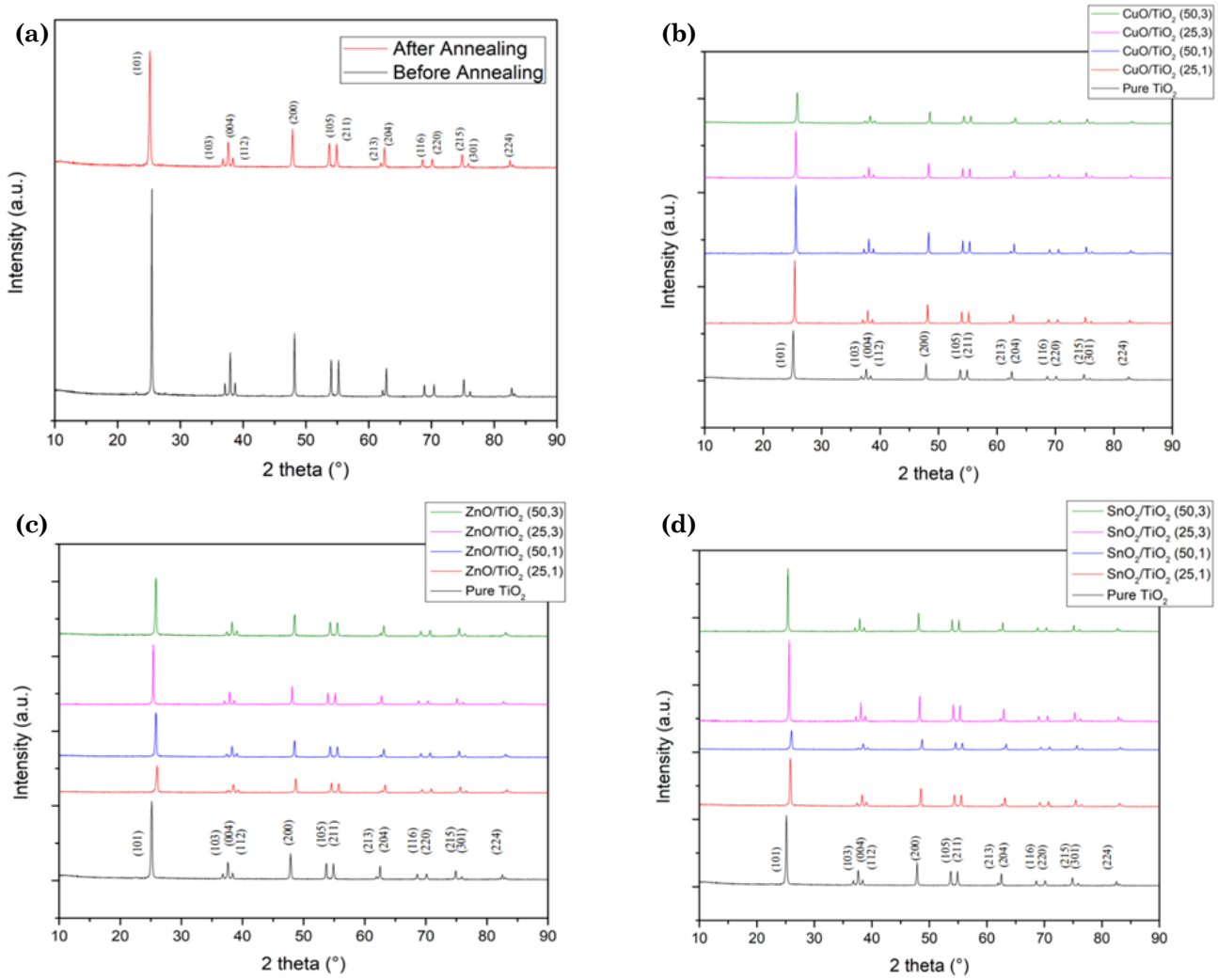

Figure 4. XRD pattern for (a) TiO_2 particles before and after annealing at 600 °C, (b) CuO/TiO_2 particles, (c) ZnO/TiO_2 particles and (d) SnO_2/TiO_2 particles.

The XRD patterns of TiO_2 and metal oxide-TiO_2 at different synthesis parameters are illustrated in Figure 4(a-d). XRD was performed on both unannealed and annealed TiO_2 particles. From the results shown in Figure 4(a), the diffraction patterns of TiO_2 particles before and after annealing were matched with ICSD 98-007-6028 (Anatase), hence both samples are in anatase form. The peaks appeared at angle 25.29°, 37.79°, 48.01°, 53.88°, 55.03°, 62.66°, 68.74°, 70.24°, 75.02°, and 82.63°, corresponding to (101), (004), (200), (105), (211), (204), (116), (220), (215), and (224), respectively. On top of that, the sharp diffraction peaks were due to the high crystallinity of both samples. Although the anatase phase could transform into a rutile phase at high temperatures [35], the XRD results indicate that heating at 600 °C in an ambient atmosphere was not sufficient for the phase transformation to take place. The overall peak intensity from TiO_2 after annealing was lower simply due to natural variation between measurements, as the overall intensity is proportional to the number of samples exposed to the X-Ray irradiation in certain slit openings, which is related to the powder packing during sample preparation.

The diffraction patterns of various CuO/TiO_2 samples, ZnO/TiO_2 samples and SnO_2/TiO_2 samples are shown in Figure 4(b-d), together with the diffraction pattern of pure TiO_2 at various synthesis parameters. It can be seen that the diffraction patterns of the metal oxide coupled TiO_2 particles showed similar peaks as the uncoupled pure TiO_2 particles, which was the anatase phase (ICSD 98-007-6028), and no other foreign peaks can be found. This was because the deposited materials present in extremely small amounts, as already been shown in the EDX results, the atomic percentages of the coupled elements (Cu, Zn, and Sn) were less than 1 at%. If the coupled material was present in very small amount, the diffraction peaks of the coupled material would not be detected due to the limitation of XRD analysis, which explains why the synthesized samples showed similar diffraction peaks as pure anatase [36].

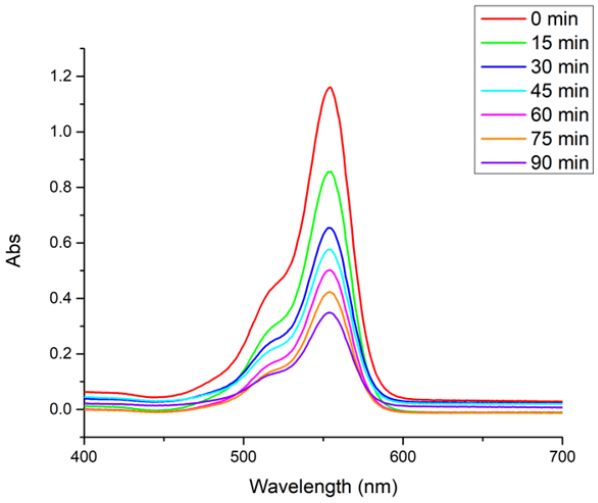

Figure 5. UV-Vis spectra of RhB solution photodegraded by uncoupled TiO_2 particles.

3.2 Photocatalytic Properties

3.2.1 The photocatalytic performance of uncoupled TiO_2 particles

The photodegradation properties of uncoupled TiO_2 particles were examined as a control. According to the Beer-Lambert Law, the concentration of a solution can be linearly proportioned to its absorbance value [37]. The concentration of RhB solution at different times of photodegradation was determined based on its absorbance peak value. Figure 5 shows the absorbance spectra of the RhB solution after vari-

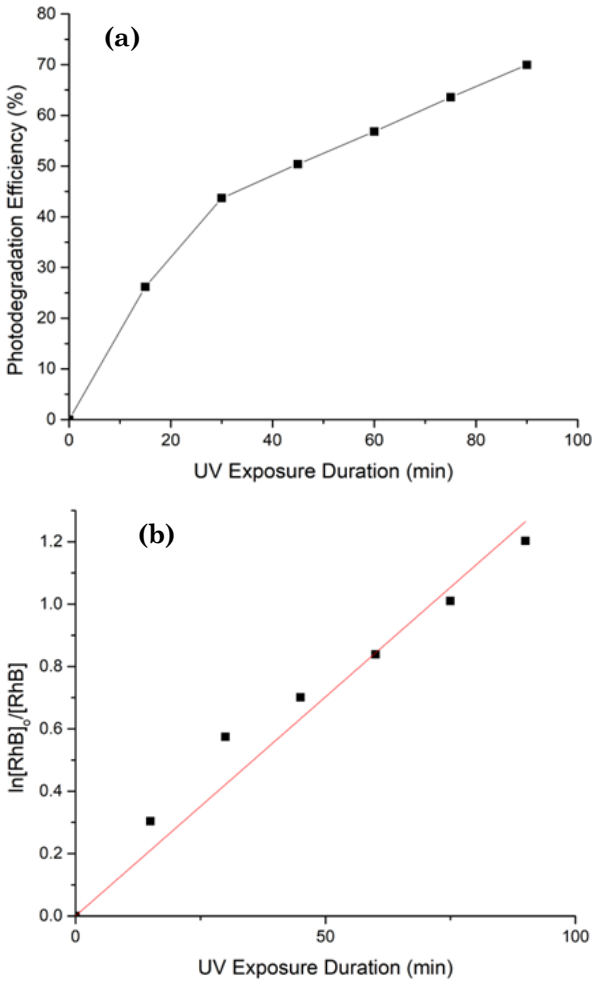

Figure 6. (a) Photodegradation efficiency by uncoupled TiO_2 particles (b) Kinetic plot of photodegradation by uncoupled TiO_2 particles.

ous UV exposure durations with the presence of uncoupled TiO_2 particles. Peak values of the absorbance spectra decreased as the exposure duration increased. According to the study of Carneiro *et al*. [38], the decrease of degradation of characteristic absorbance peak is an indication of degradation of RhB dye into oxalic acid, 2-hydroxybutanoic acid, 4-ketopentanoic acid, butanedionic acid, benxoic acid, and benzene dicarboxylic acid. Figure 6(a) shows the photodegradation efficiency of RhB solution by uncoupled TiO_2 particles under UV irradiation. 69.95% of the RhB solution has been photodegradated after 90 min of UV exposure. Figure 6(b) shows the plot of $\ln\{[RhB]_o/[RhB]\}$ vs t. A linear fitting was performed and R^2 value of 97.30% was obtained. This has shown that the photodegradation of RhB solution with uncoupled TiO_2 particles under UV irradiation followed a first-order kinetic [39]. The rate constant of the photodegradation was determined from the slope of the plot, which is 0.01258 min^{-1}.

3.2.2 The photocatalytic performance of metal oxide coupled TiO_2 particles

Figure 7(a) shows the photodegradation efficiencies of various CuO/TiO_2 samples at different exposure durations. The photodegradation efficiency of uncoupled TiO_2 particles was also included for comparison purposes. Overall, CuO/TiO_2 samples showed better photodegradation efficiencies than pure TiO_2 particles. Just like uncoupled TiO_2 particles, the results indicate the CuO/TiO_2 samples follow a first-order kinetics for RhB photodegradation. After 90 min of UV irradiation, the CuO/TiO_2 samples, which were CuO/TiO_2 (25,1), CuO/TiO_2 (50,1), CuO/TiO_2 (25,3), and CuO/TiO_2 (50,3) have degraded 89.96%, 90.29%, 90.90%, and 92.67% of RhB solution, respectively. CuO/TiO_2 (50,1), CuO/TiO_2 (25,3), and CuO/TiO_2 (50,3) showed rather similar photodegradation patterns and slightly greater photodegradation than CuO/TiO_2 (25,1). This can be explained by a higher atomic percentage of Cu in CuO/TiO_2 (50,1), CuO/TiO_2 (25,3), and CuO/TiO_2 (50,3), with 0.76 at% for the first two samples and 0.79 at% for the third sample, compared to CuO/TiO_2 (25,1) with slightly lower Cu percentage at 0.62 at%. A higher atomic percentage of Cu would indicate more TiO_2 particles were being coupled, thereby contributing to a more efficient photodegradation overall [40,41]. To better understand the effect of various parameters on the photocatalytic performance, the reaction rate constant of each sample was plotted against the methanol concentration and deposition duration, in Figure 8(a-b). For samples with the same amount of methanol concentration, the ones with a longer deposition duration have a larger rate constant, and vice versa. Once again, the rate constants were due

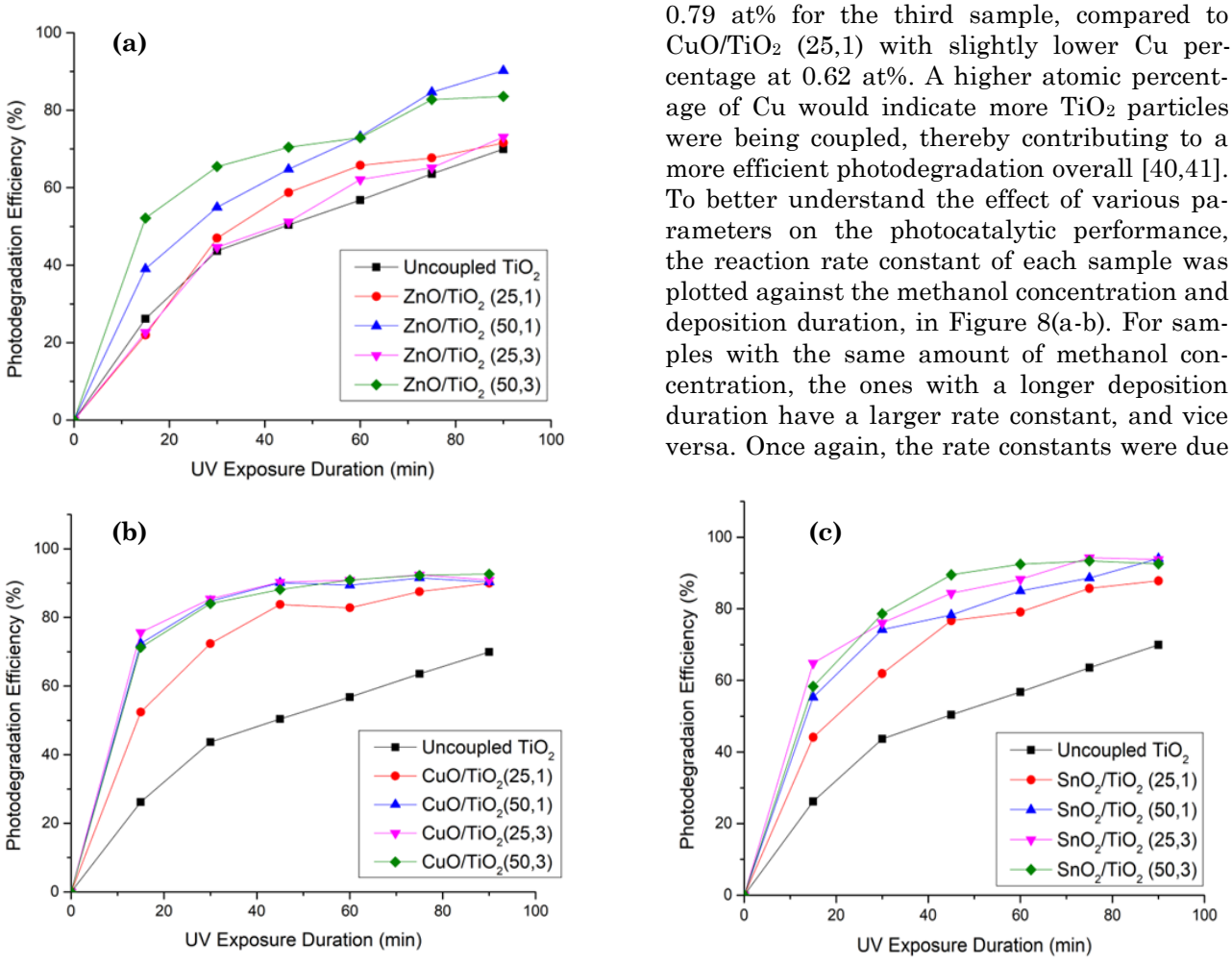

Figure 7. Photodegradation efficiencies of uncoupled TiO_2 particles and various (a) CuO/TiO_2 particles, (b) ZnO/TiO_2 particles and (c) SnO_2/TiO_2 particles.

to the respective amount of photodeposited materials.

Figure 7(b) illustrates the photodegradation efficiencies of various ZnO/TiO_2 samples and pure TiO_2 particles at different exposure durations. ZnO has almost similar band gap energy with anatase TiO_2 at around 3.3eV [23]. ZnO has hexagonal unit cell instruction called Wurtzite, as well as large exiting binding energy and large bond strength at room temperature [42]. From Figure 7(b), ZnO/TiO_2 (50,3) and ZnO/TiO_2 (50,1) have shown better photo-

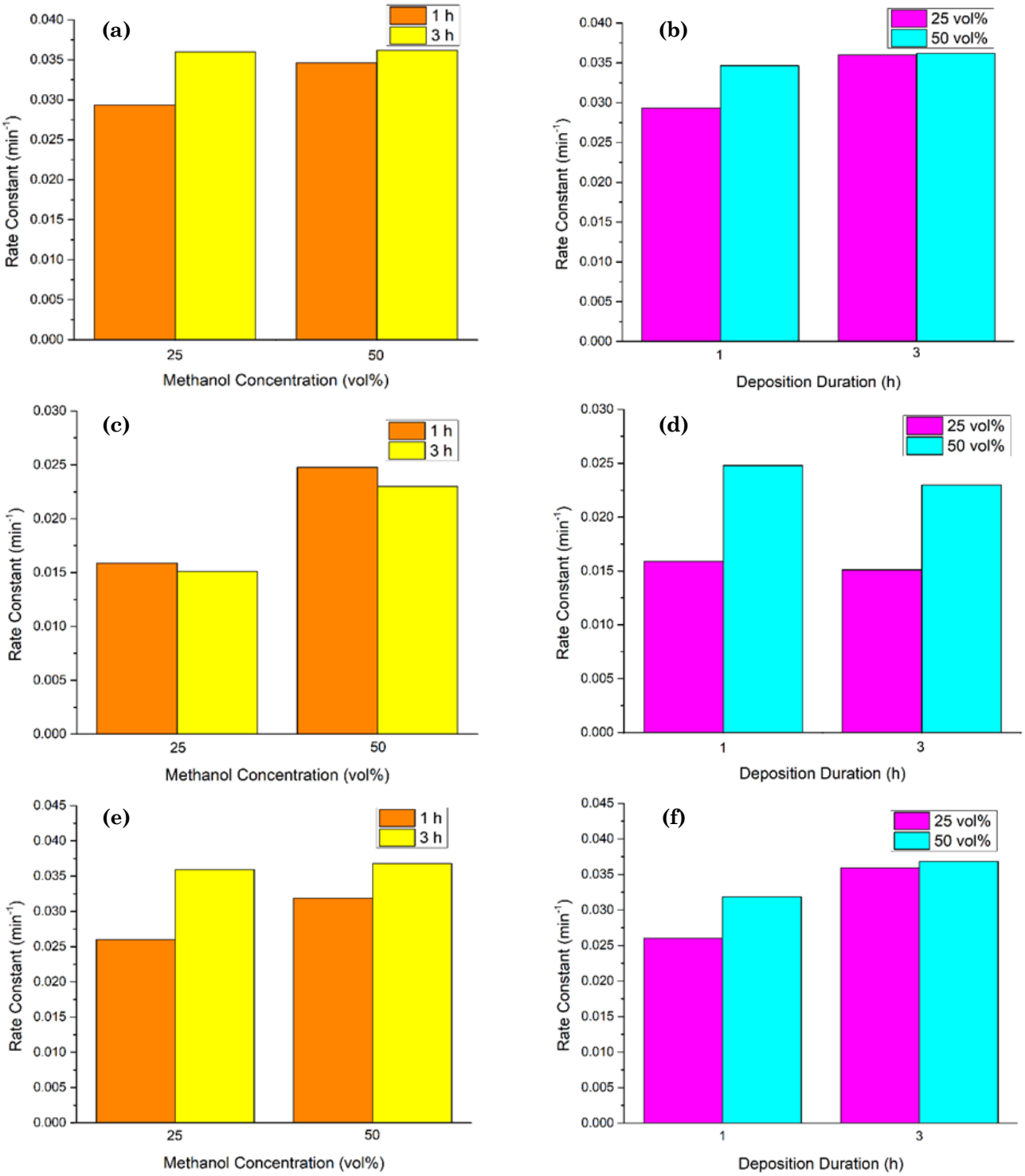

Figure 8. Photodegradation rate constants of RhB solution by various metal oxides synthesized using different (a) methanol concentration (CuO/TiO_2), (b) deposition duration (CuO/TiO_2), (c) methanol concentration (ZnO/TiO_2), (d) deposition duration (ZnO/TiO_2), (e) methanol concentration (SnO_2/TiO_2) and (f) deposition duration (SnO_2/TiO_2).

degradation efficiencies than ZnO/TiO_2 (25,1) and ZnO/TiO_2 (25,3), which only have slightly better photodegradation efficiencies than pure TiO_2 particles. After 90 min of UV irradiation, ZnO/TiO_2 (50,3) and ZnO/TiO_2 (50,1) have degraded 90.25% and 83.60% of the RhB solution, respectively. On the other hand, ZnO/TiO_2 (25,3) and ZnO/TiO_2 (25,1) have only degraded 73.07% and 71.57% of RhB solution, respectively after 90 min of UV irradiation. Similar to pure TiO_2 particles, the photodegradation of RhB solution by ZnO/TiO_2 particles followed a first-order reaction kinetics. From previous EDX analysis, the atomic percentage of Zn in ZnO/TiO_2 (25,1) and ZnO/TiO_2 (25,3) was only 0.20 at% and 0.46 at%, respectively, compared to ZnO/TiO_2 (50,1) and ZnO/TiO_2 (50,3) which have 0.57 at% and 0.98 at% of Zn, respectively. A higher atomic percentage of Zn present in the samples indicates that more Zn was being photodeposited onto the sample which was then converted to ZnO during oxidation annealing. On top of that, the results have shown that the overall photocatalytic properties of ZnO/TiO_2 samples (average rate constant of 0.0197 min^{-1}) were not as good as CuO/TiO_2 samples (average rate constant of 0.0341 min^{-1}). This indicates the charge carrier recombination prevention mechanism in CuO/TiO_2, where Cu^{2+} ions "hold" the photogenerated electrons, was much more effective than in ZnO/TiO_2 (direct charge transfer in heterojunction), resulting in better photocatalytic properties of CuO/TiO_2. This is also likely due to the small bandgap of CuO, allowing it to be excited not only by UV light but also by visible light as well, hence able to generate more charge carriers upon illumination. To visualize the effect of various coupling parameters on the photocatalytic performance of the ZnO/TiO_2 samples, the reaction rate constants of each sample were plotted against the methanol concentration and deposition duration, in Figure 8(c-d). For ZnO/TiO_2 samples synthesized with 25 vol% of methanol used, the rate constant was almost the same at 0.0159 min^{-1} and 0.0151 min^{-1}, compared to when 50 vol% of methanol was used with rate constants of 0.0248 min^{-1} and 0.0230 min^{-1}.

Figure 7(c) depicts the photodegradation efficiencies of various SnO_2/TiO_2 samples at different exposure durations with that of pure TiO_2. From the figure, the photodegradation efficiency by SnO_2/TiO_2 samples were generally better than pure TiO_2. After UV irradiation of 90 min, SnO_2/TiO_2 (50,1), SnO_2/TiO_2 (25,3), and SnO_2/TiO_2 (50,3) have degraded almost the same percentage of RhB solution, which were 94.05%, 93.79%, and 92.61%, respectively, whereas SnO_2/TiO_2 (25,1) has shown slightly lower photodegradation efficiency with 87.92% at 90 min. Based on the EDX analysis results, SnO_2/TiO_2 (25,3) and SnO_2/TiO_2 (50,3) have higher atomic percentages of Sn (0.94 at% and 1.04 at%, respectively) and thus they were expected to show greater photodegradation properties due to more coupling of SnO_2 with TiO_2 particles. However, SnO_2/TiO_2 (50,1) with a lower Sn percentage (0.41 at%) than SnO_2/TiO_2 (25,1) (0.66 at%) has displayed a greater photodegradation efficiency than SnO_2/TiO_2 (25,1). This was likely due to the unintended exposure of SnO_2/TiO_2 (50,1) containing RhB solution, to surrounding light and caused the photodegradation of RhB solution to proceed in the cuvette under visible light irradiation because coupling TiO_2 with SnO_2 will cause a red shift in band gap to the visible region [43]. To see the effect of various coupling parameters on the photocatalytic performance of the SnO_2/TiO_2 samples, the reaction rate constants of each sample were plotted against the methanol concentration and deposition duration, in Figure 8(e-f). From Figure 8(f), for a deposition duration of 3 h, the synthesized samples have almost similar photodegradation rate constants of 0.0360 min^{-1} and 0.0368 min^{-1}.

Table 2 compares the photodegradation rate constants of all samples, including the pure TiO_2 for comparison. The rate constants of CuO/TiO_2 samples (average of 0.0341 min^{-1}) are much higher than ZnO/TiO_2 samples (average of 0.0197 min^{-1}). Despite having different charge carrier recombination inhibition mechanisms, SnO_2/TiO_2 samples (direct charge

Table 2. Summary of rate constants of all samples.

Sample	Rate Constant, k (min^{-1})
CuO/TiO_2 (25,1)	0.0293
CuO/TiO_2 (50,1)	0.0347
CuO/TiO_2 (25,3)	0.0360
CuO/TiO_2 (50,3)	0.0362
ZnO/TiO_2 (25,1)	0.0159
ZnO/TiO_2 (50,1)	0.0248
ZnO/TiO_2 (25,3)	0.0151
ZnO/TiO_2 (50,3)	0.0230
SnO_2/TiO_2 (25,1)	0.0260
SnO_2/TiO_2 (50,1)	0.0319
SnO_2/TiO_2 (25,3)	0.0360
SnO_2/TiO_2 (50,3)	0.0368
Pure TiO_2	0.0141

transfer mechanism) have shown similar photocatalytic properties as CuO/TiO_2 samples with an average rate constant of 0.0327 min^{-1}, and both have shown better photocatalytic properties than ZnO/TiO_2 samples. Although SnO_2/TiO_2 particles and ZnO/TiO_2 particles both use a direct charge transfer mechanism for inhibiting charge carrier recombination, however due to the relative band position of SnO_2 and ZnO with TiO_2, the TiO_2 stores different charge carriers in each case. In the case of ZnO/TiO_2, the CB of ZnO is at a higher energy level than the CB of TiO_2, hence TiO_2 holds the photogenerated electrons from both components. On the other hand, in the case of SnO_2/TiO_2, the VB of TiO_2 is higher than the VB of SnO_2, so TiO_2 holds the photogenerated holes from both components. TiO_2 has strong adsorption properties that can hold high concentrations of target pollutant molecules close to its surface [43]. In the case of SnO_2/TiO_2, the surface of TiO_2 contains a high amount of photogenerated holes which can directly oxidize the pollutant molecules gathered around its surface, while at the same time generate hydroxyl radicals (that can degrade the pollutant molecules) through the reaction between the holes and water molecules which is abundant in the solution [44].

For ZnO/TiO_2, the photogenerated electrons in TiO_2 cannot react directly with the pollutant molecules near the TiO_2 surface. Besides, the presence of oxygen molecules in the solution is not as abundant as water molecules, hence the generation of superoxide radicals (which also can degrade the pollutant molecules) is not as frequent. The two factors mentioned above may be contributing to the less efficient photodegradation activity displayed by ZnO/TiO_2 samples compared to SnO_2/TiO_2 samples. In the end, the relative bandgap of the coupled oxide with TiO_2 is not the determining factor of the combined photocatalytic properties, instead, it is the relative positions of the CB and VB that are impactful. Among CuO/TiO_2 and SnO_2/TiO_2 samples, CuO/TiO_2 (50,3) and SnO_2/TiO_2 (50,3) have shown the best photocatalytic properties respectively due to the longer deposition time and higher concentration methanol, resulting in more deposited materials. Overall, all synthesized samples have shown better photocatalytic properties than pure TiO_2 as suggested in previous studies.

4. Conclusion

This research systematically explored the coupling of TiO_2 with various metal oxides (CuO, ZnO, and SnO_2) for enhancing the photocatalytic degradation of Rhodamine B (RhB) dye. The study encompassed a comprehensive investigation into the impact of synthesis parameters, including methanol concentration and deposition duration, on the photocatalytic performance of the coupled materials. EDX analysis has confirmed the deposition of desired materials on TiO_2 particles, however, the amount was too small to be detected by XRD analysis. Besides, the SEM image and EDX elemental composition suggested that the deposited metal oxides were likely to be in the form of particulates only. As for the photocatalytic performances, all synthesized samples have shown improved performance on the photodegradation of RhB solutions. The photodegradation of RhB solution by pure TiO_2 and synthesized samples have shown to follow first-order kinetics. The results demonstrated that CuO/TiO_2 and SnO_2/TiO_2 samples exhibited superior photocatalytic properties. The study elucidated that deposition duration and methanol concentration significantly influenced the photodeposition process, with longer durations and higher methanol concentrations resulting in enhanced photocatalytic activity. CuO/TiO_2 (50,3) and SnO_2/TiO_2 (50,3) were identified as the most effective photocatalysts, benefiting from extended deposition times and greater methanol concentrations. The findings underscore the importance of carefully choosing metal oxides and synthesis conditions to tailor photocatalytic processes for specific applications. Future work in this field may further explore the optimization of synthesis parameters and the potential for scaling up these photocatalytic systems for practical environmental applications.

Acknowledgement

The authors gratefully acknowledge the financial support of the Ministry Of Higher Education Malaysia For the Fundamental Research Grant Scheme With Project Code: FRGS/1/2022/STG05/USM/03/3 and the support from the Universiti Sains Malaysia.

CRediT Author Statement

Author Contributions: *Amna Jwad Kadem*: Investigation, Methodology, Roles/Rewriting - original draft. *Zhuang Min Tan*: Conceptualization, Data curation, Formal analysis, Investigation, Methodology, Roles/Writing - original draft. *Mohana Suntharam Nanthini*: Conceptualization, Data curation, Formal analysis. *Swee-Yong Pung*: Conceptualization, Formal analysis, Funding acquisition, Resources, Validation, Writing - review & editing. *Ramakrishnan Sivakumar*: Conceptualization, Formal analysis, Investigation, Project administration, Resources, Supervision, Validation, Writing - review & editing. All authors have read and agreed to the published version of the manuscript.

References

[1] Syuhadah, N. (2017). Environmental contamination by batik wastewater and the potential application of activated carbon from pineapple waste for wastewater treatment. *Thesis*, Universiti Sains Malaysia.

[2] Rajlaxmi, R., Gupta, N., Behere, R.P., Layek, R.K., Kuila, B.K. (2021). Polymer nanocomposite membranes and their application for flow catalysis and photocatalytic degradation of organic pollutants. *Materials Today Chemistry*, 22, 100600. DOI: 10.1016/j.mtchem.2021.100600.

[3] Sun, Z., Vollpracht, A., van der Sloot, H.A. (2019). pH dependent leaching characterization of major and trace elements from fly ash and metakaolin geopolymers. *Cement and Concrete Research*, 125, 105889. DOI: 10.1016/j.cemconres.2019.105889.

[4] Kulkarni, S.G. (2013). Removal of organic matter from domestic waste water by adsorption. *International Journal of Science, Engineering and Technology Res*earch, 2, 1836–1839.

[5] Bhatti, Z.A., Mahmood, Q., Raja, I.A., Malik, A.H., Khan, M.S., Wu, D. (2011). Chemical oxidation of carwash industry wastewater as an effort to decrease water pollution. *Physics and Chemistry of the Earth*, 36(9–11), 465–469. DOI: 10.1016/j.pce.2010.03.022.

[6] Ghernaout, D. (2017). Short Communication: Requiring Reverse Osmosis Membranes Modifications – An Overview. *American Journal of Chemical Engineering*, 5(4), 81. DOI: 10.11648/j.ajche.20170504.15.

[7] Bai, N., Liu, X., Li, Z., Ke, X., Zhang, K., Wu, Q. (2021). High-efficiency TiO_2/ZnO nanocomposites photocatalysts by sol–gel and hydrothermal methods. *Journal of Sol-Gel Science and Technology*, 99(1), 92–100. DOI: 10.1007/s10971-021-05552-8.

[8] Xu, Q., Zhang, L., Yu, J., Wageh, S., Al-Ghamdi, A.A., Jaroniec, M. (2018). Direct Z-scheme photocatalysts: Principles, synthesis, and applications. *Materials Today,* 21(10), 1042–1063. DOI: 10.1016/j.mattod.2018.04.008.

[9] Ameta R., Solanki M.S., Benjamin S., Ameta S.C. (2023). Photocatalysis. In S.C. Ameta, R. Ameta *Advanced Oxidation Processes for Wastewater Treatment: Emerging Green Chemical Technology*. Institute of Physics Publishing. DOI: 10.1016/B978-0-12-810499-6.00006-1.

[10] Oshida, Y. (2013). Oxidation and Oxides. In Y. Oshida *Bioscience and Bioengineering of Titanium Materials*. Elsevier B.V. DOI: 10.1016/B978-0-444-62625-7.00004-2.

[11] Dontsova, T.A., Kutuzova, A.S., Bila, K.O., Kyrii, S.O., Kosogina, I.V., Nechyporuk, D.O. (2020). Enhanced Photocatalytic Activity of TiO_2/SnO_2 Binary Nanocomposites. *Journal of Nanomaterials*, 2020, 8349480. DOI: 10.1155/2020/8349480.

[12] Chen, X., Mao, S.S. (2007). Titanium dioxide nanomaterials: Synthesis, properties, modifications and applications. *Chemical Reviews,* 107(7), 2891–2959. DOI: 10.1021/cr0500535.

[13] Ohtani, B. (2010). Photocatalysis A to Z-What we know and what we do not know in a scientific sense. *Journal of Photochemistry and Photobiology C: Photochemistry Reviews*, 11(4), 157–178. DOI: 10.1016/j.jphotochemrev.2011.02.001.

[14] Hosseini-Sarvari, M., Jafari, F., Mohajeri, A., Hassani, N. (2018). Cu_2O/TiO_2 nanoparticles as visible light photocatalysts concerning $C(sp_2)$-P bond formation. *Catalysis Science and Technology*, 8(16), 4044–4051. DOI: 10.1039/c8cy00822a.

[15] Karami, A. (2010). Iranian Chemical Society. Synthesis of TiO_2 Nano Powder by the Sol-Gel Method and Its Use as a Photocatalyst. *Journal of the Iranian Chemical Society*, 7, S154–S160. DOI: 10.1007/BF03246194.

[16] Zhang, F.B., Li, H.L. (2007). Hydrothermal synthesis of TiO_2 nanofibres. *Materials Science and Engineering C*, 27(1), 80–82. DOI: 10.1016/j.msec.2006.02.001.

[17] Mirmasoomi, S.R., Ghazi, M.M., Galedari, M. (2017). Photocatalytic degradation of diazinon under visible light using TiO_2/Fe_2O_3 nanocomposite synthesized by ultrasonic-assisted impregnation method. *Separation and Purification Technology*, 175, 418–427. DOI: 10.1016/j.seppur.2016.11.021.

[18] Fan, Y., Zhang, N., Zhang, L., Shao, H., Wang, J., Zhang, J., Cao, C. (2013). Co_3O_4-coated TiO_2 nanotube composites synthesized through photo-deposition strategy with enhanced performance for lithium-ion batteries. *Electrochimica Acta*, 94, 285–293. DOI: 10.1016/j.electacta.2013.01.114.

[19] Jiang, C., Zhang, L., Gao, F., Huang, X., Lei, R., Ye, Y., Yuan, J., Liu, P. (2020). Promoting photocatalytic hydrogen production by a core-shell CdS@MoO: X photocatalyst connected by an S-Mo "bridge." *Catalysis Science and Technology*, 10(5), 1368–1375. DOI: 10.1039/c9cy02492a.

[20] Zhang, H., Banfield, J.F. (2000). Understanding polymorphic phase transformation behavior during growth of nanocrystalline aggregates: Insights from TiO_2. *Journal of Physical Chemistry B*, 104(15), 3481–3487. DOI: 10.1021/jp000499j.

[21] Carp, O., Huisman, C.L., Reller, A. (2004). Photoinduced reactivity of titanium dioxide. *Progress in Solid State Chemistry*, 32(1–2), 33–177. DOI: 10.1016/j.progsolidstchem.2004.08.001.

[22] Hernández-Alonso, M.D., Fresno, F., Suárez, S., Coronado, J.M. (2009). Development of alternative photocatalysts to TiO_2: Challenges and opportunities. *Energy and Environmental Science*, 2(12), 1231–1257. DOI: 10.1039/b907933e.

[23] Das, A., Kumar, P. M., Bhagavathiachari, M., Nair, R.G. (2020). Hierarchical ZnO-TiO_2 nanoheterojunction: A strategy driven approach to boost the photocatalytic performance through the synergy of improved surface area and interfacial charge transport. *Applied Surface Science*, 534, 147321. DOI: 10.1016/j.apsusc.2020.147321.

[24] Yamamoto, M., Minoura, Y., Akatsuka, M., Ogawa, S., Yagi, S., Yamamoto, A., Yoshida, H., Yoshida, T. (2020). Comparison of platinum photodeposition processes on two types of titanium dioxide photocatalysts. *Physical Chemistry Chemical Physics*, 22(16), 8730–8738. DOI: 10.1039/c9cp06988g.

[25] Sefardjella, H., Boudjema, B., Kabir, A., Schmerber, G. (2013). Structural and photoluminescence properties of SnO_2 obtained by thermal oxidation of evaporated Sn thin films. *Current Applied Physics*, 13(9), 1971–1974. DOI: 10.1016/j.cap.2013.08.017.

[26] Castrejón-Sánchez V.H., Solís A.C., López R., Encarnación-Gomez C., Morales F.M., VargasO. S., Sánchez G.V. (2019). Thermal oxidation of copper over a broad temperature range: towards the formation of cupric oxide (CuO). *Materials Research Express*, 6, 075909. DOI: 10.1088/2053-1591/ab1662.

[27] Nerle, U., Rabinal, M.K. (2013). Thermal Oxidation of Copper for Favorable Formation of Cupric Oxide (CuO) Semiconductor. *IOSR Journal of Applied Physics*, 5, 1-7. DOI: 10.9790/4861-0510107.

[28] Raship, N.A., Sahdan, M.Z., Adriyanto, F., Nurfazliana, M.F., Bakri, A.S. (2017). Effect of annealing temperature on the properties of copper oxide films prepared by dip coating technique. *AIP Conference Proceedings*, 1788, 030121. DOI: 10.1063/1.4968374.

[29] Choudhary, S., Sarma, J.V.N., Pande, S., Ababou-Girard, S., Turban, P., Lepine, B., Gangopadhyay, S. (2018). Oxidation mechanism of thin Cu films: A gateway towards the formation of single oxide phase. *AIP Advances*, 8, 055114. DOI: 10.1063/1.5028407.

[30] Catauro, M., Tranquillo, E., Dal Poggetto, G., Pasquali, M., Dell'Era, A., Ciprioti, S.V. (2018). Influence of the heat treatment on the particles size and on the crystalline phase of TiO_2 synthesized by the sol-gel method. *Materials*, 11(12), 2364. DOI: 10.3390/ma11122364.

[31] Toe, M.Z., Pung, S.Y., Le, A.T., Yaccob, K.A., Matsuda, A., Tan, W.K., Han, S.S. (2021). Morphology and optical properties of ZnO nanorods coupled with metal oxides of various bandgaps by photo-oxidation. *Journal of Luminescence*, 229, 117649. DOI: 10.1016/j.jlumin.2020.117649.

[32] Mousa, H.M., Alenezi, J.F., Mohamed, I.M.A., Yasin, A.S., Hashem, A.F.M., Abdal-hay, A. (2021). Synthesis of TiO_2@ZnO heterojunction for dye photodegradation and wastewater treatment. *Journal of Alloys and Compounds*, 886, 161169. DOI: 10.1016/j.jallcom.2021.161169.

[33] Chenthamarakshan, C.R., Rajeshwar, K. (2000). Photocatalytic reduction of divalent zinc and cadmium ions in aqueous TiO_2 suspensions: An interfacial induced adsorption-reduction pathway mediated by formate ions. *Electrochemistry Communications*, 2, 527–530. DOI: 10.1016/S1388-2481(00)00078-3.

[34] Chenthamarakshan, C.R., Yang, H., Ming, Y., Rajeshwar, K. (2000). Photocatalytic reactivity of zinc and cadmium ions in UV-irradiated titania suspensions. *Journal of Electroanalytical Chemistry*, 494, 79–86. DOI: 10.1016/S0022-0728(00)00374-0.

[35] Zhang, Q., Li, C. (2020). High temperature stable anatase phase titanium dioxide films synthesized by mist chemical vapor deposition. *Nanomaterials*, 10(5), 0911. DOI: 10.3390/nano10050911.

[36] Shifu, C., Lei, C., Shen, G., Gengyu, C. (2005). The preparation of coupled WO_3/TiO_2 photocatalyst by ball milling. *Powder Technology*, 160(3), 198–202. DOI: 10.1016/j.powtec.2005.08.012.

[37] Tahergorabi, M., Esrafili, A., Shirzad-Siboni, M., Kermani, M. (2020). Photodegradation of catechol in water over magnetically separable Fe_3O_4/TiO_2 composite photocatalysts. *International Journal of Environmental Analytical Chemistry*, 102(16), 4575–4593. DOI: 10.1080/03067319.2020.1785441.

[38] Carneiro, J.O., Samantilleke, A.P., Parpot, P., Fernandes, F., Pastor, M., Correia, A., Luís, E.A., Chivanga Barros, A.A., Teixeira, V. (2016). Visible light induced enhanced photocatalytic degradation of industrial effluents (Rhodamine B) in aqueous media using TiO_2 nanoparticles. *Journal of Nanomaterials*, 2016, 4396175. DOI: 10.1155/2016/4396175.

[39] Kaur, H., Kaur, R. (2014). Removal of Rhodamine-B dye from aqueous solution onto Pigeon Dropping: Adsorption, Kinetic, Equilibrium, and Thermodynamic Studies. *Journal of Materials and Environmental Sciences*, 5(6), 1830–1838.

[40] Li, G., Gray, K.A. (2007). The solid-solid interface: Explaining the high and unique photocatalytic reactivity of TiO_2-based nanocomposite materials. *Chemical Physics*, 339(1–3), 173–187. DOI: 10.1016/j.chemphys.2007.05.023.

[41] Bessekhouad, Y., Robert, D., Weber, J.V. (2005). Photocatalytic activity of Cu_2O/TiO_2, Bi_2O_3/TiO_2 and $ZnMn_2O_4/TiO_2$ heterojunctions. *Catalysis Today*, 101(3–4), 315–321. DOI: 10.1016/j.cattod.2005.03.038.

[42] Mohammadi, H., Ghorbani, M. (2018). Synthesis photocatalytic TiO_2/ZnO nanocomposite and investigation through anatase, wurtzite and $ZnTiO_3$ phases antibacterial behaviors. *Journal of Nano Research*, 51, 69–77. DOI:10.4028/www.scientific.net/JNanoR.51.69.

[43] Hou, L.R., Yuan, C.Z., Peng, Y. (2007). Synthesis and photocatalytic property of SnO2/TiO_2 nanotubes composites. *Journal of Hazardous Materials*, 139(2), 310–315. DOI: 10.1016/j.jhazmat.2006.06.035

[44] Campo, C.M., Rodríguez, J.E., Ramírez, A.E. (2016). Thermal behaviour of romarchite phase SnO in different atmospheres: a hypothesis about the phase transformation. *Heliyon*, *2*(5), e00112. DOI: 10.1016/j.heliyon.2016.e00112.